

# Magnetic excitations in the weakly coupled spin dimers and chains material $\text{Cu}_2\text{Fe}_2\text{Ge}_4\text{O}_{13}$

T. Masuda,\* A. Zheludev, and B. Sales

Condensed Matter Sciences Division, Oak Ridge National Laboratory, Oak Ridge, Tennessee 37831-6393, USA

S. Imai<sup>†</sup> and K. Uchinokura<sup>‡</sup>

Department of Advanced Materials Science, The University of Tokyo, 5-1-5, Kashiwa-no-ha, Kashiwa 277-8581, Japan

S. Park<sup>§</sup>

NIST Center for Neutron Research, National Institute of Standards and Technology, Gaithersburg, Maryland 20899, USA

(Received 2 June 2005; revised manuscript received 8 August 2005; published 28 September 2005)

Magnetic excitations in a weakly coupled spin dimers and chains compound  $\text{Cu}_2\text{Fe}_2\text{Ge}_4\text{O}_{13}$  are measured by inelastic neutron scattering. Both structure factors and dispersion of low-energy excitations up to 10 meV energy transfer are well described by a semiclassical spin wave theory involving interacting  $\text{Fe}^{3+}(S=5/2)$  chains. Additional dispersionless excitations are observed at higher energies, at  $\hbar\omega=24$  meV, and associated with singlet-triplet transitions within  $\text{Cu}^{2+}$  dimers. Both types of excitations can be understood by treating weak interactions between the  $\text{Cu}^{2+}$  and  $\text{Fe}^{3+}$  subsystems at the level of the mean-field random phase approximation. However, this simple model fails to account for the measured temperature dependence of the 24 meV mode.

DOI: [10.1103/PhysRevB.72.094434](https://doi.org/10.1103/PhysRevB.72.094434)

PACS number(s): 75.10.Jm, 75.25.+z, 75.50.Ee

## I. INTRODUCTION

The ground states of low-dimensional magnets are strongly affected by quantum spin fluctuation. In so-called quantum spin liquids spin correlation remains short range even at zero temperature, and the excitation spectrum is gapped. This disorder is relatively robust and such systems resist long-range ordering even in the presence of residual three-dimensional interactions or anisotropy. In contrast, gapless low-dimensional magnets are very sensitive to external perturbations that can easily drive them toward long-range ordering. New physics is found in bicomponent systems that combine these two distinct types of low-dimensional spin networks. An example is  $\text{R}_2\text{BaNiO}_5$  materials where Haldane spin chains weakly interact with magnetic rare earth ions.<sup>1-3</sup> More recently, we reported the discovery and study of the quantum ferrimagnet  $\text{Cu}_2\text{Fe}_2\text{Ge}_4\text{O}_{13}$ .<sup>4,5</sup> We showed that this compound can be viewed as a system of antiferromagnetic (AF) Cu dimers that weakly interact with almost classical  $\text{Fe}^{3+}$  chains. This weak coupling leads to a rather unusual *cooperative* ordering phase transition at low temperatures.

The crystal structure of  $\text{Cu}_2\text{Fe}_2\text{Ge}_4\text{O}_{13}$  is monoclinic  $P2_1/m$  with  $a=12.101$  Å,  $b=8.497$  Å,  $c=4.869$  Å, and  $\beta=96.131^\circ$ .<sup>5</sup> The arrangement of magnetic ions and likely exchange pathways is shown in Fig. 1(a).  $\text{Fe}^{3+}$  ions form crankshaft-shaped chains that run in the  $b$  direction. These chains are separated by  $\text{GeO}_4$  tetrahedra in the  $c$  direction. The  $\text{Cu}^{2+}$  dimers are located in between  $\text{Fe}^{3+}$  chains along the  $a$  direction. Simultaneous cooperative long-range magnetic ordering of the two magnetic subsystems occurs at 40 K.<sup>5</sup> The magnetic structure is roughly collinear, with spins lying in the crystallographic  $a$ - $c$  plane. In addition, there are small out-of-plane spin components (canting). The saturation magnetic moment on  $\text{Cu}^{2+}$  ions is anomalously small, being suppressed by residual quantum fluctuations in

the dimers:  $m_{\text{Cu}}=0.38(4)\mu_B$ . This suggests that the coupling  $J_{\text{Cu-Fe}}$  between the Cu dimers and the Fe subsystem is weak compared to intradimer AF interactions  $J_{\text{Cu}}$ . The pairs of Cu spins remain in a spin-singlet state that is only partially polarized by interactions with the long-range order in the Fe subsystem. The data collected in preliminary inelastic neutron scattering experiments for energy transfers up to 10 meV could be well explained by fluctuations of  $\text{Fe}^{3+}$  spins alone. The  $\text{Fe}^{3+}$  spins form weakly coupled  $S=5/2$  chains, the corresponding effective exchange constants being  $J_{\text{Fe}}=1.60(2)$  meV,  $J'_{\text{Fe}}=0.12(1)$  meV, as shown in Fig. 1. These values are consistent with rough estimates of exchange constants based on magnetic susceptibility data:  $J_{\text{Fe}}=1.7$  meV,  $J_{\text{Cu}}=25$  meV. To date, no excitations associated with the Cu dimers could be identified.

While the very nature of the crankshaft-shaped chains implies some alternation of bond strength, we find no evidence thereof in the measured dispersion curves. In fact, they are well reproduced by a model involving uniform magnetic Fe chains with weak interchain interactions along the  $c$  direction. In the remainder of this work we shall therefore disregard the bond alternation and assume the Fe chains to be magnetically uniform.

In the present paper we report a more detailed inelastic neutron scattering study of  $\text{Cu}_2\text{Fe}_2\text{Ge}_4\text{O}_{13}$ . Our main result is an observation of a complete separation of energy scales for  $\text{Cu}^{2+}$ - and  $\text{Fe}^{3+}$ -centered magnetic excitations. An analysis of the intensity pattern for low-energy spin waves allows us to unambiguously associate them with the dynamics of  $S=5/2$  chains. In addition, separate narrowband excitation originating from Cu subsystem is observed at higher-energy transfers. The layout of the paper will be as follows. In Sec. II we will describe the characteristics of our samples and experimental setups. Section III describes the results for low-energy excitations in single-crystal samples, as well as measurements of the much weaker high-energy excitations in a

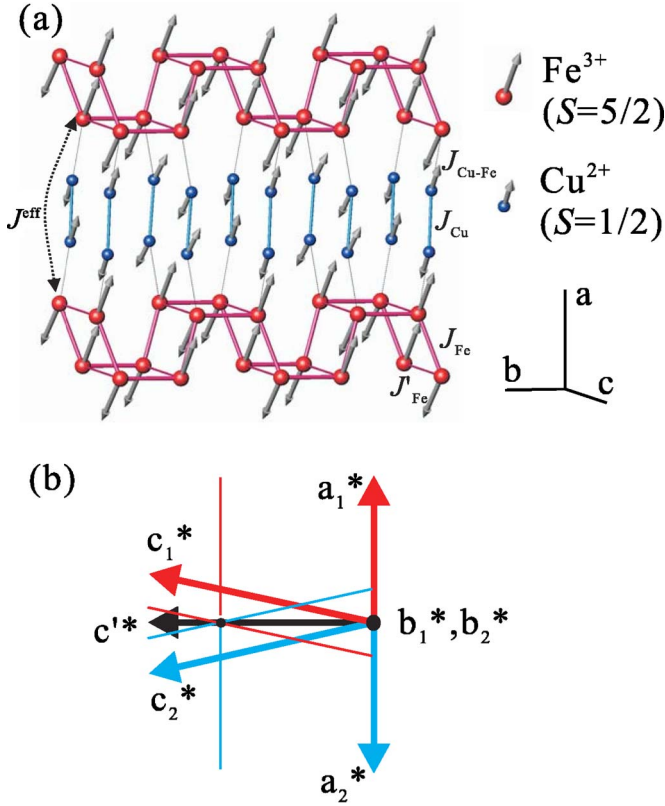


FIG. 1. (Color online) (a) A schematic view of the crystal structure of  $\text{Cu}_2\text{Fe}_2\text{Ge}_4\text{O}_{13}$ . Only magnetic ions are shown. Arrows symbolize the spin structure in the magnetically ordered phase. Possible exchange pathways are also shown. (b) Relative orientations of reciprocal-lattice vectors for the two domains in bulk crystalline samples with twinning.

large-volume powder sample. In Sec. IV we shall interpret the observed separation of energy scales by a mean-field random phase approximation (MF RPA) treatment of interactions between  $\text{Cu}^{2+}$  and  $\text{Fe}^{3+}$  spins. The discussion and conclusion will be given in Secs. V and VI, respectively.

## II. EXPERIMENT

High-quality single crystals with the dimension of  $3 \times 4 \times 35 \text{ mm}^3$  were grown by the floating zone method. All samples were found to be twinned. The two twins share a common  $(b, c)$  plane, the monoclinic structure allowing two independent orientations of the  $a$  axis. In reciprocal space the domains share a common  $(a^*, b^*)$  plane, but have distinct  $c^*$  axes, as illustrated in Fig. 1(b). Two separate single crystals were coaligned to obtain a larger sample of cumulative mosaic spread  $0.44^\circ$ . For single-crystal inelastic neutron scattering experiments we exploited three different setups. Setup 1 employed the SPINS cold neutron spectrometer at the NIST Center for Neutron Research (NCNR). The scattering plane was defined by the  $b^*$  and the bisector  $c'^*$  of the  $c^*$  axes in the two crystallographic domains, as shown in Fig. 1(b). The direction of  $c'^*$  is the same as that of the  $c$  axis in the real space. In this geometry the scattering planes are *the same* in both domains. It is convenient to define  $c'^* \equiv c^* \cos(\beta$

$-90^\circ$ ). The momentum transfer in the scattering plane of the spectrometer is then indexed by Miller indices  $h'$ ,  $k'$ , and  $l'$  of a fictitious orthorhombic structure. For the two domains  $h = \pm(c'^*/a^*)l' \tan(\beta - 90^\circ)$ ,  $k = k'$  and  $l = l'$ . Since  $\beta$  is close to  $90^\circ$ ,  $h$  is almost zero for most measurements using setup 1, where  $l$  is small. In setup 2 the scattering plane was  $(a^*, b^*)$ , which is also common for the two domain types. In both setups we used (guide)-80'-80'-(open) collimation with a Be filter positioned after the sample and a fixed final energy  $E_f = 5$  or 3 meV. The data were collected at  $T = 1.4$  K using a standard He-flow cryostat.

Intensity was the main limiting factor for studies of higher-energy magnetic excitations. To maximize sample volume the measurements were performed on a 50 g polycrystalline  $\text{Cu}_2\text{Fe}_2\text{Ge}_4\text{O}_{13}$  powder that was prepared by the solid state reaction method. This experiment was performed on the HB3 three-axis spectrometer at HFIR with 48'-40'-60'-120' collimations and a Pyrolytic graphite filter after the sample (setup 3). The final neutron energy was fixed at  $E_f = 14.7$  meV. A closed-cycle refrigerator was used to achieve low temperatures.

Setup 4 was used for wide surveys in reciprocal space on single crystals. We employed the HB1 thermal neutron spectrometer at the High Flux Isotope Reactor at ORNL. The scattering plane was  $(a^*, b^*)$ , as in setup 2. The collimation was 48'-40'-40'-240'. Neutrons with  $E_f = 13.5$  meV were used in conjunction with a pyrolytic graphite filter positioned after the sample. The experiments in setup 3 were performed at  $T = 6.4$  K maintained by a closed-cycle He refrigerator.

## III. EXPERIMENTAL RESULTS

### A. Low energies

In this section we concentrate on the low-energy excitations at energy transfers up to 10 meV. As was explained in our preliminary report<sup>5</sup> and will be discussed in detail below, this part of the spectrum can be associated with conventional spin waves from the Fe subsystem. The Cu dimers only provide an effective Fe-Fe interaction, but contribute nothing to the dynamics at low energies.

Typical energy scans at  $\mathbf{q} = (0 \ k \ 0.5)$  measured using setup 1 are shown in Fig. 2. White and gray circles correspond to data collected with  $E_f = 5$  and 3 meV, respectively. Well-defined resolution-limited peaks are observed in the entire Brillouin zone. Solid lines are Gaussian fits to the data after a subtraction of a linear background. The excitation energy is a minimum at the magnetic zone center at  $\mathbf{q} = (0 \ 2.0 \ 0.5)$ . A small gap of about 1.6 meV is observed at this wave vector. The apparent shoulder structure can be attributed to a splitting of the spin wave branch into two components with somewhat different gap energies. The gaps are most likely anisotropy related. The zone-boundary energy at  $\mathbf{q} = (0 \ 3.0 \ 0.5)$  is about 9 meV. The dispersion relation was obtained by Gaussian fits to individual scans and is shown in Fig. 3(a). The  $k$  dependence of the measured energy-integrated peak intensity is plotted in symbols in Fig. 3(b). The intensity scales roughly as  $1/\omega$ . The inset in Fig. 3(a) is a sketch of the dispersion relation of mode I that is derived in Sec. IV.

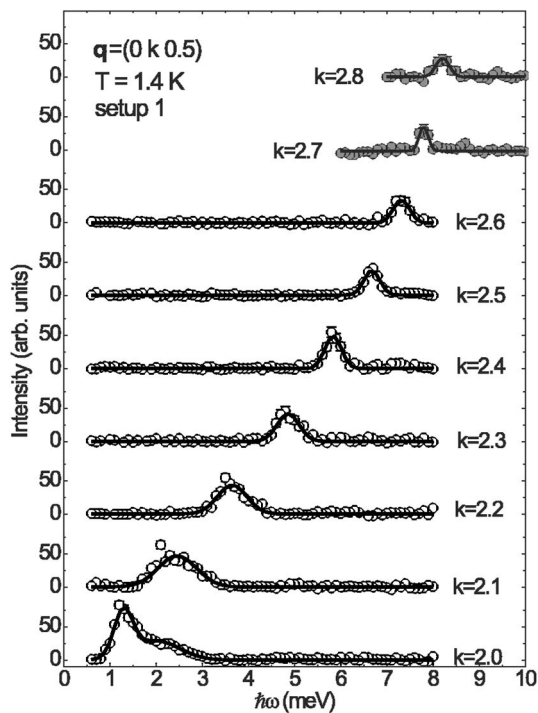


FIG. 2. Energy scans collected in  $\text{Cu}_2\text{Fe}_2\text{Ge}_4\text{O}_{13}$  for momentum transfers  $\mathbf{q}=(0 k 0.5)$ . White and gray circles correspond to measurements with  $E_f=5$  and 3 meV, respectively. Solid lines are Gaussian fits.

Energy scans at  $\mathbf{q}=(0 2.0 l)$  and  $(0 2.9 l)$  are shown in Fig. 4. Constraints on experimental geometry prevented us from reaching the more symmetric  $(0 3.0 l)$  reciprocal-space rods at higher energy transfers. These two sets of data reveal two distinct excitation branches, that are strongest near even and odd  $k$  values, respectively. The former branch is dispersive along the  $c$  axis, while the latter is almost flat. Dispersion relations and the integrated intensity plots for both modes were obtained using Gaussian fits and are shown in Figs. 5(a) and 5(b). Even for the more dispersive lower-energy branch the boundary energy along the  $c^*$  direction is only about 5 meV: about half of that in the  $b^*$  direction.

No dispersion of low-energy excitations could be detected along the  $a^*$  direction. This is illustrated by the energy scans collected on the  $(h 2.0 0)$  reciprocal-space rod using setup 2 (Fig. 6). Two peaks are observed at 5 and 9 meV, respectively. The excitation energies are plotted in Fig. 7(a). Interestingly, the peak intensity is strongly dependent on  $h$ , as shown in Fig. 7(b).

From the data presented above one can immediately conclude that the most relevant magnetic interactions are within the  $\text{Fe}^{3+}$  layers, parallel to the  $(b, c)$  plane. Interlayer coupling along the  $a$  direction, which involves the  $\text{Cu}^{2+}$  dimer coupling, is considerably weaker.

### B. Higher-energy excitations

The model that we previously proposed for  $\text{Fe}_2\text{Cu}_2\text{Ge}_4\text{O}_{13}$  (Ref. 5) implies a separation of energy scales of spin-wave-like excitations on the Fe subsystem and triplet excitations of

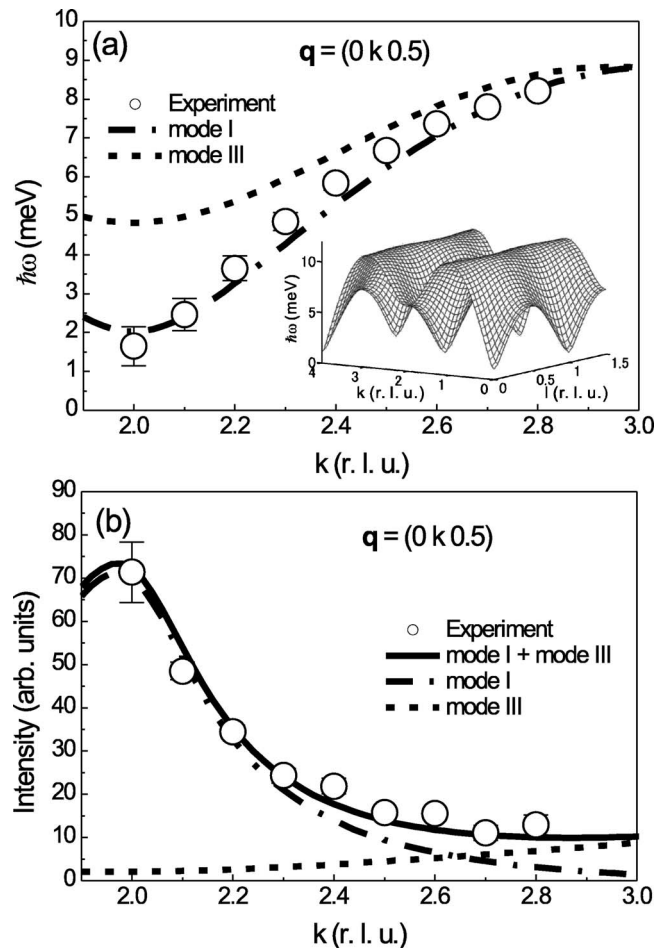


FIG. 3. Measured energies (a) and integrated intensities (b) of magnetic excitations as a function of momentum transfer along the  $b^*$  direction (symbols). Lines are as described in the text.

the Cu dimers. From magnetic susceptibility measurements we have estimated the intradimer exchange constant to be around 25 meV. Due to the small sample size, in single-crystal experiments we failed to observe any clear magnetic inelastic features in this energy transfer range. To search for the Cu-triplet mode we performed additional measurements on a large-size powder sample by employing the setup 3 experimental configuration.

The powder data collected at  $T=12$  K are summarized in the false color plot in Fig. 8(a). The data were obtained by combining 17 separate constant- $q$  scans. For each such scan a linear background was subtracted from the measured intensity. Figure 8(a) clearly shows a narrow excitation band at  $\hbar\omega \sim 24$  meV. The measured intensity of the 24 meV peak decreases with the increase of  $q$ , as expected for magnetic scattering. The observed energy width at  $q=2.3 \text{ \AA}^{-1}$  is somewhat larger than experimental resolution, but still small compared to the central energy [Fig. 8(b)]. Such energy dependence in powder samples typically indicates a narrow dispersion bandwidth (see, for example, Refs. 6 and 7). The observed spectrum is consistent with the excitations originating from the structural Cu dimers, indicated by the thick solid bonds in Fig. 1(a). However, the momentum transfer range covered in the experiment, especially at  $|q| \rightarrow 0$ , is in-

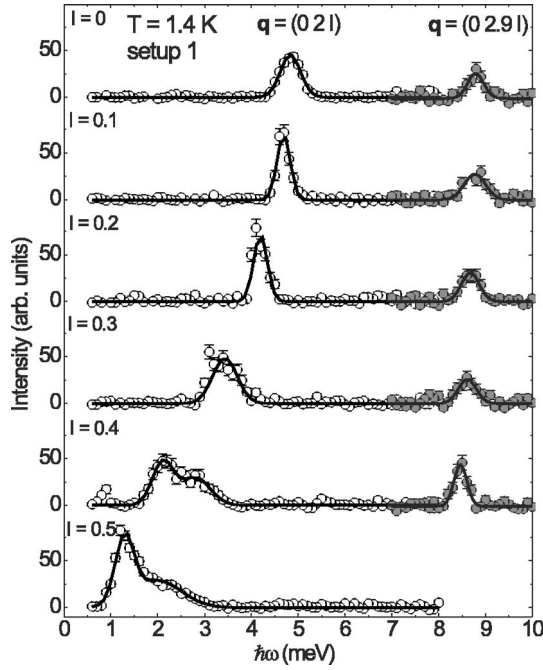


FIG. 4. Energy scans collected in  $\text{Cu}_2\text{Fe}_2\text{Ge}_4\text{O}_{13}$  for several momentum transfers along the  $c^*$  direction. Symbols and lines are as in Fig. 2.

sufficient for a more detailed analysis of the structure factor. In particular, the size of the dimers cannot be independently extracted from the experimental data.

To obtain additional information on the 24 meV excitation we studied its temperature dependence at  $q=2.3 \text{ \AA}^{-1}$ . The main challenge was dealing with a large background that originates from (i) temperature-independent scattering, including spurious scattering from an “accidental” Bragg powder line at 24.8 meV and (ii) temperature-dependent phonon scattering. These two contributions can be removed from the data if one assumes that the useful magnetic signal is relatively weak and/or temperature independent above  $T=200 \text{ K}$ . This would indeed be true if the magnetic scattering originated from effectively isolated Cu dimers with an intradimer exchange constant of 24 meV. The phonon contribution, which is assumed to scale with the Bose factor, is thus estimated from comparing scans at  $T=300 \text{ K}$  and  $T=200 \text{ K}$ . It is then appropriately scaled and subtracted from all scans, leaving only the true magnetic signal and the  $T$ -independent background. The two cannot, in principle, be reliably separated. However, we can follow the *change* in magnetic signal from  $T=200 \text{ K}$  by using the phonon-subtracted  $T=200 \text{ K}$  scan as “background.”

The result of this elaborate background subtraction is plotted in Fig. 9. The well-defined peak seen at low temperature broadens progressively with increasing  $T$  and practically disappears at  $T \gtrsim 40 \text{ K}$ . In this range there also seems to be a downward shift in the peak’s central energy.

#### IV. ANALYSIS

##### A. Separation of energy scales

To understand the dynamics of the coupled  $\text{Fe}^{3+}$  and  $\text{Cu}^{2+}$  subsystems we shall make the central assumption that the

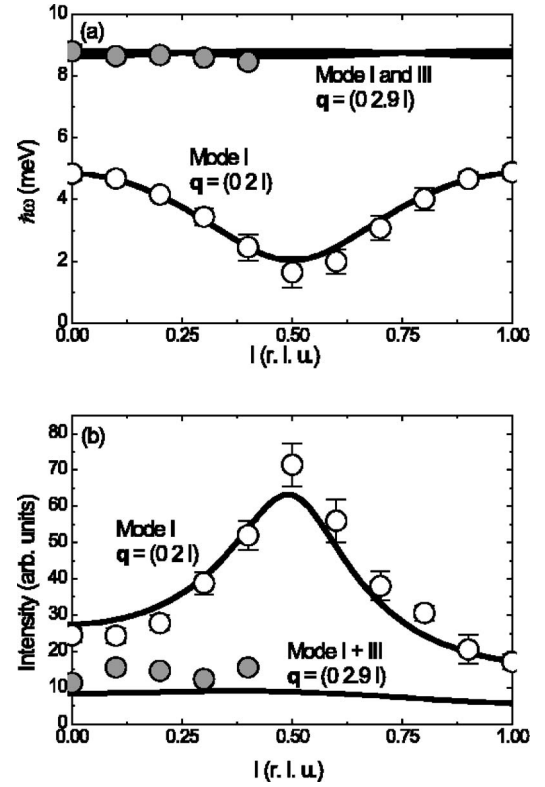


FIG. 5. Measured energies (a) and integrated intensities (b) of magnetic excitations as a function of momentum transfer along the  $c^*$  direction. The solid and open circles correspond to the higher- and lower-energy branches, respectively. Lines are as described in the text.

exchange constant  $J_{\text{Cu}}$  that binds pairs of  $\text{Cu}^{2+}$  spins into AF dimers is the largest energy scale in the system. Under these circumstances the degrees of freedom associated with Cu spins can be effectively integrated out at low energies. Indeed, the isolated  $\text{Cu}^{2+}$  subsystem has a spin singlet ground state and a large energy gap  $\Delta=J_{\text{Cu}}$ . At  $\hbar\omega \ll \Delta$  it lacks any intrinsic dynamics, i.e., its dynamic susceptibility is purely real and almost energy independent. In the spirit of RPA, from the point of view of  $\text{Fe}^{3+}$  spins, the Cu dimers merely act as a polarizable medium that can transfer magnetic interactions between the Fe layers. The staggered spin susceptibility of each  $S=1/2$  dimer being  $2/(J_{\text{Cu}})$ , this effective coupling, labeled as  $J_{\text{eff}}$  in Fig. 1 is given by

$$J_{\text{eff}}^{\text{eff}} = J_{\text{Cu-Fe}}^2 / (2J_{\text{Cu}}). \quad (1)$$

Thus, to a good approximation, the low-energy spin dynamics of  $\text{Fe}_2\text{Cu}_2\text{Ge}_4\text{O}_{13}$  is simply that of the  $\text{Fe}^{3+}$  subsystem with an additional exchange coupling. From the experiment, where no dispersion of spin waves could be observed along the  $a$  axis, the effective exchange constant must be rather small. Nevertheless, as explained in our previous paper,<sup>5</sup> it is absolutely crucial in completing a three-dimensional spin network and allowing long-range magnetic ordering at a nonzero temperature.

At high energy transfers, comparable to the Cu dimer gap, it is the  $\text{Fe}^{3+}$  degrees of freedom that can be effectively in-

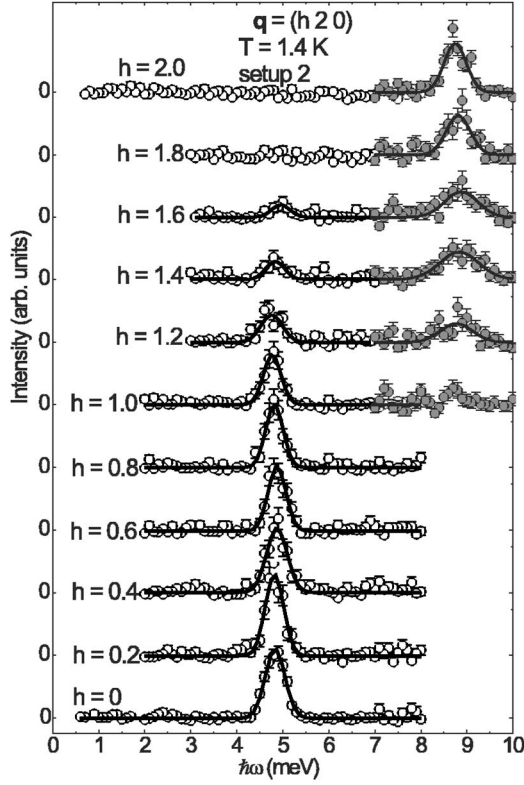


FIG. 6. Energy scans measured in  $\text{Cu}_2\text{Fe}_2\text{Ge}_4\text{O}_{13}$  for momentum transfers  $\mathbf{q}=(h\ 2\ 0)$ . Symbols and lines are as in Fig. 2.

tegrated out. At  $T < T_N$  their effect is reduced to producing a *static* staggered exchange spin field that acts on the  $\text{Cu}^{2+}$  spins and is proportional to the ordered  $\text{Fe}^{3+}$  moment:

$$h^{\text{Cu}} = \langle S_{\text{Fe}} \rangle J_{\text{Cu-Fe}}. \quad (2)$$

In our approximation at high energy transfers  $\text{Cu}_2\text{Fe}_2\text{Ge}_4\text{O}_{13}$  behaves as a collection of (possibly interacting) Cu dimers in an effective staggered field.<sup>5</sup>

### B. Spin waves and dynamic structure factor for low energies

As explained above, the low-energy spectrum of  $\text{Cu}_2\text{Fe}_2\text{Ge}_4\text{O}_{13}$  can be understood by considering the Fe subsystem in isolation, and even  $J_{\text{eff}}$  can be ignored for its smallness. For the magnetically ordered state the dynamic structure factor of such a system can be calculated using conventional spin wave theory (SWT). For simplicity we shall assume a collinear magnetic structure, ignoring the small canting of the  $\text{Fe}^{3+}$  spins out of the  $(a, c)$  plane. In the first step of our analysis we fitted the dispersion relation with the coupled *alternating* chains by numerical method.<sup>8</sup> The obtained exchange parameters were the same for both alternating bonds in our experimental error. For the further calculation of the structure factor we can approximately employ magnetically uniform chains that will give us intuitive physical meanings of the observed modes.

There are four Fe ions in each unit cell of  $\text{Cu}_2\text{Fe}_2\text{Ge}_4\text{O}_{13}$ , even though we assume *magnetically* uniform chains and the topology of exchange interactions defined by  $J_{\text{Fe}}$  and  $J'_{\text{Fe}}$  in

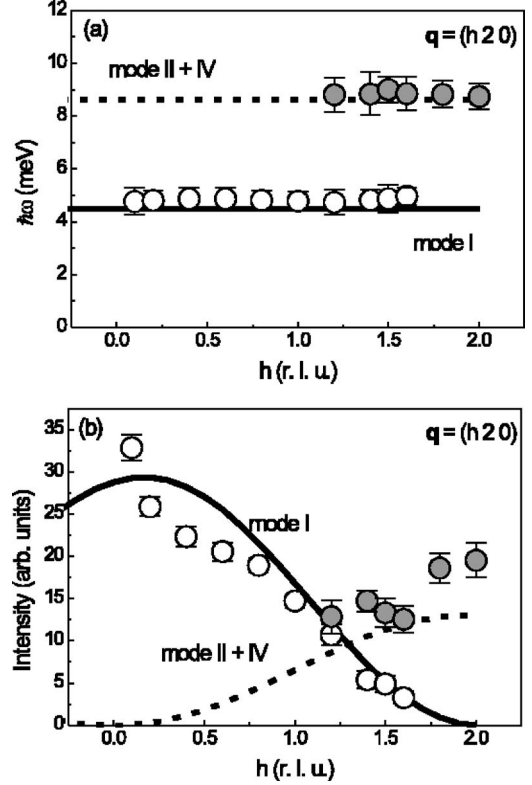


FIG. 7. (a) Measured energies (a) and integrated intensities (b) of magnetic excitations as a function of momentum transfer along the  $a^*$  direction. Symbols and lines are as in Fig. 5.

Fig. 1 is that of a regular Bravais lattice. The relation between real lattice and the magnetically equivalent lattice is illustrated in Fig. 10. The actual structure factor  $S(\mathbf{q}, \omega)$  and  $S_0(\mathbf{q}, \omega)$  for the equivalent lattice is *exactly* related as follows:

$$\begin{aligned} S(\mathbf{q}, \omega) = & S_0(\mathbf{q}, \omega) \cos^2 2\pi\delta_a h \cos^2 2\pi\delta_b k \\ & + \frac{1}{2} S_0(\mathbf{q} + (0, 1, 0), \omega) (1 + \sin^2 2\pi\delta_a h \sin^2 2\pi\delta_b k) \\ & + S_0(\mathbf{q} + (0, 2, 0), \omega) \cos^2 2\pi\delta_a h \sin^2 2\pi\delta_b k \\ & + \frac{1}{2} S_0(\mathbf{q} + (0, 3, 0), \omega) (1 + \sin^2 2\pi\delta_a h \sin^2 2\pi\delta_b k), \end{aligned} \quad (3a)$$

$$\delta_a = 0.1239, \quad \delta_b = 0.0629. \quad (3b)$$

Here  $\delta_a$  and  $\delta_b$  are the displacements of  $\text{Fe}^{3+}$  ions from high-symmetry positions, as shown in Fig. 1(b).

The SWT dynamic structure factor for a collinear antiferromagnet on a Bravais lattice is well known:<sup>9</sup>

$$S_0(\mathbf{q}, \omega) = (u_{\mathbf{q}} + v_{\mathbf{q}})^2 \delta(\hbar\omega_{\mathbf{q}} - \hbar\omega), \quad (4a)$$

$$u_{\mathbf{q}}^2 = \frac{S(\hbar\omega_{\mathbf{q}} + 2Sj(0))}{\hbar\omega_{\mathbf{q}}}, \quad (4b)$$

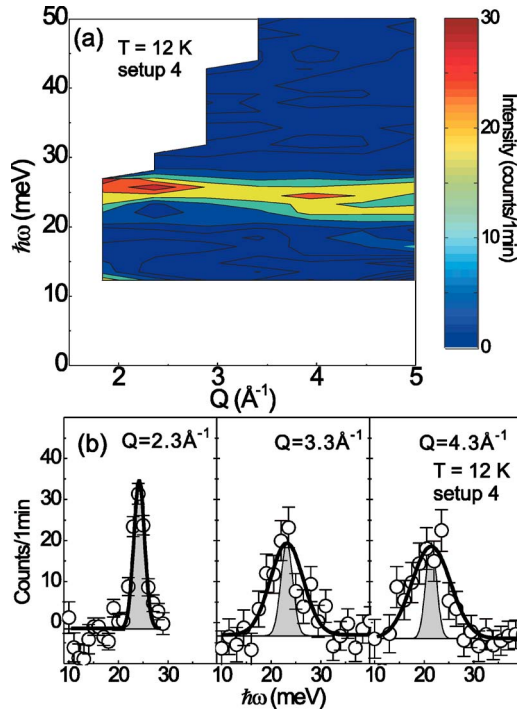


FIG. 8. (Color online) (a) False-color plot of inelastic intensity measured in  $\text{Cu}_2\text{Fe}_2\text{Ge}_4\text{O}_{13}$  powder samples as a function of energy and momentum transfer. (b) Typical energy scans measured at  $T = 12 \text{ K}$  for different momentum transfers. Heavy solid lines are Gaussian fits. The shaded Gaussians represent experimental energy resolution.

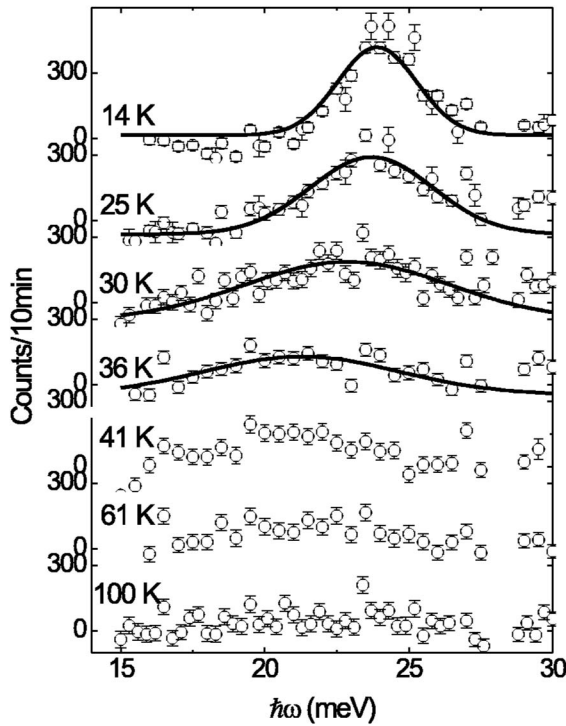


FIG. 9. Typical energy scans at measured in  $\text{Cu}_2\text{Fe}_2\text{Ge}_4\text{O}_{13}$  powder at  $q = 2.3 \text{\AA}^{-1}$  for different temperatures. Solid lines are Gaussian fits. The background has been subtracted, as explained in the text.

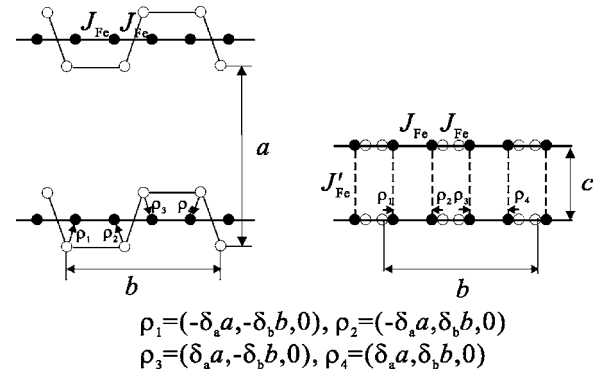


FIG. 10. Spatial arrangement of  $\text{Fe}^{3+}$  sites in the structure of  $\text{Cu}_2\text{Fe}_2\text{Ge}_4\text{O}_{13}$  (open circles) and an equivalent Bravais lattice of spins (solid circles).

$$u_{\mathbf{q}} v_{\mathbf{q}} = -\frac{2S^2 j(\mathbf{q})}{\hbar\omega_{\mathbf{q}}}, \quad (4c)$$

$$\hbar\omega_{\mathbf{q}} = S\sqrt{j(0)^2 - j(\mathbf{q})^2 + \Delta^2}. \quad (4d)$$

Here  $j(\mathbf{q})$  is the Fourier transform of exchange interactions, and  $\Delta$  empirically accounts for the anisotropy gap. In our particular case of the  $\text{Fe}^{3+}$  subsystem in  $\text{Cu}_2\text{Fe}_2\text{Ge}_4\text{O}_{13}$  we have

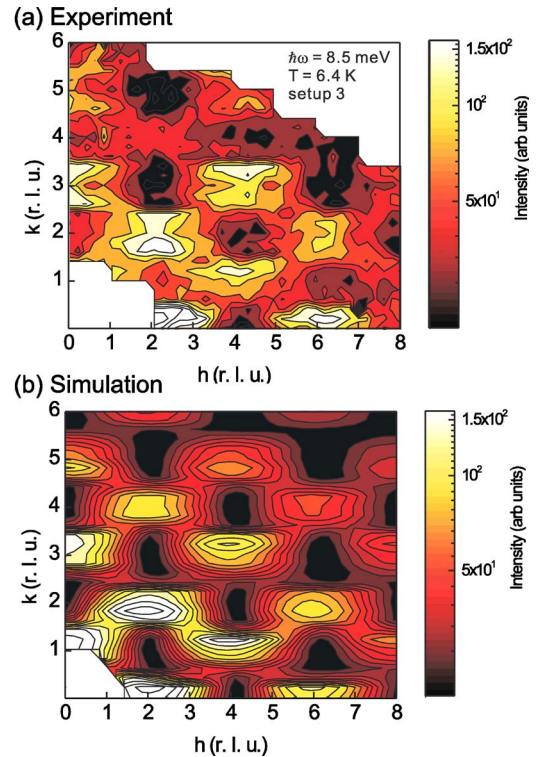


FIG. 11. (Color online) (a) Constant energy scans at  $\hbar\omega = 8.5 \text{ meV}$  in wide  $\mathbf{q} = (hk0)$  range. (b) Simulation based on our model cross section convoluted with the experimental resolution function.

TABLE I. Exchange parameters for  $\text{Cu}_2\text{Fe}_2\text{Ge}_4\text{O}_{13}$ .

$J_{\text{Fe}}$	$J'_{\text{Fe}}$	$J^{\text{eff}}$	$J_{\text{Cu-Fe}}$	$J_{\text{Cu}}$
1.60(2) meV	0.12(1) meV	0.13(4) meV	2.54(3) meV	24.(2) meV

$$j(\mathbf{q}) = 2 \left( J_{\text{Fe}} \cos \frac{\pi}{2} k + J'_{\text{Fe}} \cos 2\pi l \right). \quad (5)$$

The cross section for inelastic neutron scattering from spin waves is given by

$$\frac{d^2\sigma}{d\Omega dE} \propto |F(\mathbf{q})|^2 \left[ 1 + \left( \frac{q_y}{q} \right)^2 \right] \langle n_{\mathbf{q}} + 1 \rangle S(\mathbf{q}, \omega). \quad (6)$$

In this formula  $F(\mathbf{q})$  is the magnetic form factor for  $\text{Fe}^{3+}$ ,  $\langle n_{\mathbf{q}} \rangle$  is the Bose factor, and  $q_z$  is the projection of the scattering vector onto the direction of ordered  $\text{Fe}^{3+}$  moments.

### C. Fits to data

The model cross section given by Eq. (6) can accurately reproduce the observed low-energy spectra in  $\text{Cu}_2\text{Fe}_2\text{Ge}_4\text{O}_{13}$ . Due to the presence of four terms in Eq. (3), there are four distinct spin wave branches, which we shall denote as modes I through IV, respectively. The dispersion relation given by Eq. (4d) was fitted to the experimental data shown in Figs. 3(a) and 5(a) using a least-squares algorithm. A good fit is obtained with  $J_{\text{Fe}}=1.60$  meV,  $J'_{\text{Fe}}=0.12$  meV, and  $\Delta=2.02$  meV. The result is shown in lines in Figs. 3(a) and 5(a). With these parameters our model also agrees well with the measured dispersion (or, rather, absence thereof) along the  $a$  axis, as shown in Fig. 7(a).

What is important is that not only the energies but also the intensities of the observed excitations are well reproduced by our model. Calculated intensities for each mode are shown in lines in Figs. 3(b), 5(b), and 7(b). In cases where experimental energy resolution is insufficient to resolve individual branches, combined intensities of a couple of modes are shown. This quantitative agreement between the measured and observed structure factors confirms that the scattering is indeed due to  $\text{Fe}^{3+}$  spins. An excellent illustration of this was obtained by mapping out the scattering intensity in a wide  $\mathbf{q}$  range using setup 4, as shown in Fig. 11(a). These data correspond to a fixed energy transfer  $\hbar\omega=8.5$  meV, and have a characteristic checkerboard pattern. Our spin wave model with the parameters quoted above reproduces this behavior very well, as shown in Fig. 11(b). In this calculation the model cross section was numerically convoluted with the known experimental resolution function. The apparent periodicity along  $k$  is due to a steep dispersion that takes the excitations in and out of the probed energy range. However, the periodicity along  $h$  is related to the trigonometric coefficients in Eq. (3a). These, in turn, are determined by the geometry of the crankshaft-shaped  $\text{Fe}^{3+}$  chains in  $\text{Cu}_2\text{Fe}_2\text{Ge}_4\text{O}_{13}$ .

### V. DISCUSSION AND CONCLUSION

As demonstrated above, the low-energy spin dynamics of  $\text{Cu}_2\text{Fe}_2\text{Ge}_4\text{O}_{13}$  is well described by an effective spin wave theory for the  $\text{Fe}^{3+}$  spin chains. Based on the available data it is impossible to unambiguously associate the observed 24 meV mode with the  $\text{Cu}^{2+}$  dimers. However, much confidence in this assumption can be drawn from a recent study of  $\text{Cu}_2\text{Sc}_2\text{Ge}_4\text{O}_{13}$ .<sup>10</sup> In this *isostructural* compound<sup>11</sup> only the  $\text{Cu}^{2+}$  ions are magnetic. Indeed the magnetic susceptibility was fitted by  $S=1/2$ -dimers with  $J_{\text{Cu}} \sim 26$  meV.<sup>10</sup> The consistency of the energy scales strongly suggests that the origin of the high-energy excitation is the same for both isostructural compounds.

We can now estimate all the relevant exchange interactions in the system. Using Eq. (2) in combination with the staggered susceptibility of an isolated antiferromagnetic dimer, from the known saturation moments  $\langle S_{\text{Cu}} \rangle = 0.18(8)$  and  $\langle S_{\text{Fe}} \rangle = 1.77(4)$  for  $\text{Cu}^{2+}$  and  $\text{Fe}^{3+}$ , respectively,<sup>5</sup> we get  $J_{\text{Cu-Fe}} = 2.54(3)$  meV. The effective coupling is then  $J^{\text{eff}} = 0.13(4)$  meV. The results for all exchange parameters are summarized in Table I.

Our model for  $\text{Cu}_2\text{Fe}_2\text{Ge}_4\text{O}_{13}$  is qualitatively consistent with the observed slight increase of the energy of the Cu-dimer mode with decreasing temperature. Indeed, the gap energy of isolated dimers, as that of other gapped systems, is known to increase with the application of a staggered field.<sup>12,13</sup> In  $\text{Cu}_2\text{Fe}_2\text{Ge}_4\text{O}_{13}$  this field is generated by the ordered moment on the  $\text{Fe}^{3+}$  sites, and at  $T < T_N$  increases proportionately to  $\langle S_{\text{Fe}} \rangle$ . In spite of the qualitatively consistent explanation, the observed  $T$  dependence of the 24 meV mode is quantitatively different from that for isolated dimers. In the case of isolated dimers, the intensity would remain almost constant below  $T=40$  K. Moreover, the peak would remain sharp at all temperatures. The discrepancy may be related to intrinsic limitations of the MF RPA approach, and merits further investigation. In particular, it is tempting to somehow associate the observed emergence and sharpening of the 24 meV inelastic peak with the onset of long-range order.

Our data bring solid quantitative support to the concept of separation of energy scales in the mixed-spin quantum antiferromagnet  $\text{Cu}_2\text{Fe}_2\text{Ge}_4\text{O}_{13}$ . Using a simple MF RPA approach we are able to determine all the relevant exchange interactions. However, certain features of the temperature dependence of spin excitations require further theoretical and experimental study.

### ACKNOWLEDGMENTS

Work at ORNL was carried out under Contract No. DE-AC05-00OR22725, U.S. Department of Energy. Experiments at NIST were supported by the NSF through Grants No. DMR-0086210 and No. DMR-9986442.

\*Present address: International Graduate School of Arts and Sciences, Yokohama City University, 22-2, Seto, Kanazawa-ku, Yokohama city, Kanagawa, 236-0027, Japan. Electronic address: tmasuda@yokohama-cu.ac.jp

†Present address: Semiconductor R & D Center, Yokohama R & D Laboratories, The Furukawa Electric Co., Ltd., Japan.

‡Present address: The Institute of Physical and Chemical Research (RIKEN), Wako, Saitama 351-0198, Japan.

§Present address: HANARO Center, Korea Atomic Energy Research Institute, Daejeon, South Korea.

<sup>1</sup>A. Zheludev, J. P. Hill, and D. J. Buttrey, *Phys. Rev. B* **54**, 7216 (1996).

<sup>2</sup>A. Zheludev, E. Ressouche, S. Maslov, T. Yokoo, S. Raymond, and J. Akimitsu, *Phys. Rev. Lett.* **80**, 3630 (1998).

<sup>3</sup>J. V. Alvarez, R. Valenti, and A. Zheludev, *Phys. Rev. B* **65**, 184417 (2002).

<sup>4</sup>T. Masuda, B. C. Chakoumakos, C. L. Nygren, S. Imai, and K.

Uchinokura, *J. Solid State Chem.* **176**, 175 (2003).

<sup>5</sup>T. Masuda, A. Zheludev, B. Grenier, S. Imai, K. Uchinokura, E. Ressouche, and S. Park, *Phys. Rev. Lett.* **93**, 077202 (2004).

<sup>6</sup>A. Zheludev, G. Shirane, Y. Sasago, M. Hase, and K. Uchinokura, *Phys. Rev. B* **53**, 11642 (1996).

<sup>7</sup>T. Masuda, A. Zheludev, H. Kageyama, and A. Vasiliev, *Europhys. Lett.* **63**, 757 (2003).

<sup>8</sup>A. W. Sáenz, *Phys. Rev.* **125**, 1940 (1962).

<sup>9</sup>See, for example, S. W. Lovesey, *Theory of Neutron Scattering from Condensed Matter* (Clarendon, Oxford, 1984), Vol. 2.

<sup>10</sup>T. Masuda *et al.* (unpublished).

<sup>11</sup>G. J. Redhammer and G. Roth, *J. Solid State Chem.* **177**, 2714 (2004).

<sup>12</sup>Th. Jolicœur and O. Golinelli, *Phys. Rev. B* **50**, 9265 (1994).

<sup>13</sup>S. Ma, D. H. Reich, C. Broholm, B. J. Sternlieb, and R. W. Erwin, *Phys. Rev. B* **51**, R3289 (1995).